Finite-Element Method Coupled With Method of Lines for the Analysis of Planar or Quasi-Planar Transmission Lines

Hao-Hui Chen, *Member, IEEE*

***Abstract*—A full-wave analysis incorporating the finite-element method (FEM) and the method of lines (MoL) is presented in this paper to investigate a planar or quasi-planar transmission-line structure containing complex geometric/material features. For a transmission-line structure being considered, the regions containing complex media are modeled by the FEM while those consisting of simple media with simple geometry are analyzed using the MoL. From the field solutions calculated by MoL, the boundary conditions are constructed. The boundary integrals involved in finite-element analysis are then carried out using these boundary conditions. Since the finite-element analysis is employed only in the complex parts of the structures, while other parts are handled by the MoL, this approach not only retains the major advantage of the FEM in simulating complex structures but also becomes more efficient than the conventional finite-element analysis. Good agreement between the calculated results and those reported in the available literature is obtained and thus validates the present approach. Furthermore, proficient computational efficiency of this method is demonstrated by examining its convergence property. Finally, a number of relevant transmission-line structures are analyzed to illustrate the applications of this approach.**

***Index Terms*—Complex features, finite-element method (FEM), method of lines (MoL), planar/quasi-planar transmission lines.**

I. INTRODUCTION

PLANAR or quasi-planar transmission lines such as microstrip lines, coplanar waveguides, and dielectric waveguides have been widely used in microwave and millimeter-wave integrated circuit systems. In some applications, the transmission lines may be designed with complex geometric parameters and/or contain inhomogeneous materials. For example, abrupt or inhomogeneously doped semiconductor substrates have been used to improve the quality factor and the slow-wave characteristics of metal–insulator–semiconductor (MIS) transmission lines [1]–[4]. Conductors with finite thickness and nonrectangular edge profile, which result from the underetching or electrolytical growth during the fabrication process, are often present in monolithic microwave integrated circuits (MMICs) or high-speed interconnects. To obtain an accurate and reliable prediction of the circuit performance, the effects due to the variation of conductor thickness and edge profile should be carefully considered [5]–[8]. In addition, micromachined microwave transmission lines such as membrane microstrips [9], [10], micromachined coplanar waveguides [11]–[13], V- and W-shaped shielded microstrip lines [14], and overlay coplanar waveguides [15], [16], have been developed recently for microwave and millimeter-wave applications. The micromachined transmission lines, which are designed using selectively etched substrates or partially elevated conductors, can be fabricated in various microwave circuit systems to increase the circuit performance and reduce size and cost [17].

Rigorous full-wave analysis of transmission-line structures containing complex geometric/material features can be carried out using several numerical techniques. There have been papers reported that using the finite-element method (FEM) [1], method of lines (MoL) [2], transmission-line matrix (TLM) method [3], and mode-matching technique in conjunction with Galerkin's method [4], [18], [19] to investigate the propagation characteristics of microstrips and coplanar waveguides fabricated on an inhomogeneous substrate. In addition, the effects of conductor thickness and edge profile on transmission properties were studied by the boundary integral equation method [5], the spectral-domain approach (SDA) [6], and FEM [7], [8]. Moreover, the conformal mapping method (CMM) [11], the finite-difference time-domain (FDTD) technique [10], and FEM [14] have been applied to analyze various micromachined transmission lines and circuits.

Of all the various numerical methods, discretization approaches like FEM or FDTD may be the most powerful and versatile techniques for handling waveguide problems having complex geometric/material parameters. By discretizing the problem domain appropriately, these approaches can effectively model complex geometric and material features. However, when highly accurate results are pursued, they normally require large computer memory and will entail massive CPU time consumption.

On the other hand, the MoL is regarded as a special discretization technique but more efficient in computation as compared with other regular discretization approaches. For a two-dimensional (2-D) problem, the domain is first partitioned into layers. Differential equations are then discretized in one direction (the direction parallel to the interfaces of layers) while solving the other one analytically. The formulation using the semianalytical procedure would substantially reduce the number of unknowns and save a great deal of computing time. However, this method requires the materials in each layer to be at least piecewise uniform along the discretization direction because it uses several

---

Manuscript received January 21, 2002; revised October 22, 2002. This work was supported by the National Science Council, Taiwan, R.O.C., under Grant NSC-91-2213-E-211-008.

The author is with the Department of Electronic Engineering, Huafan University, Taipei, Taiwan, R.O.C. (e-mail: hhchen@huafan.hfu.edu.tw).

Digital Object Identifier 10.1109/TMTT.2003.808623

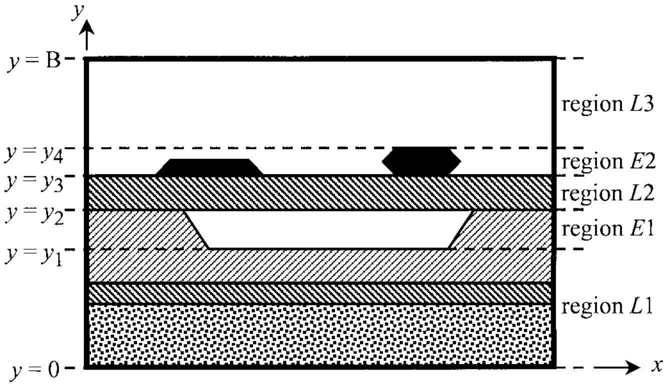

Fig. 1. Transmission-line structure containing complex geometric/material features.

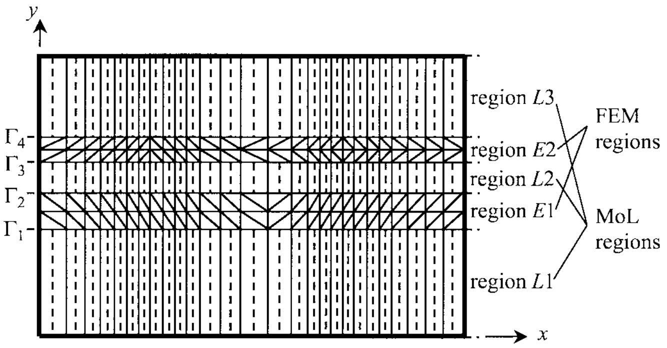

Fig. 2. Discretization schemes for the FEM–MoL analysis of the structure shown in Fig. 1. The FEM regions are discretized by triangular elements. The MoL regions are discretized by e-lines and h-lines (solid and dashed vertical lines in MoL regions).

straight lines to divide the problem domain. When a complex structure is involved, this method may not be applicable.

In this paper, a full-wave approach incorporating the FEM and the MoL (FEM–MoL) is proposed for the analysis of planar or quasi-planar transmission lines. In the FEM–MoL analysis of a structure containing complex geometric/material features (such as the example shown in Fig. 1), the regions containing complex features (such as nonrectangular metal strips) are investigated by the FEM. The MoL is then applied to analyze the regions consisting of simple media with simple geometry (such as the stratified homogeneous substrate layers). From the field solutions calculated by the MoL, the boundary conditions over the boundaries of the complex regions are constructed. Afterwards, the boundary integrals involved in finite-element analysis can be carried out using these boundary conditions.

In this FEM–MoL analysis, since the complex regions are modeled by the FEM, advantages associated with the FEM in simulating complex features are retained. Furthermore, due to the fact that 2-D discretization of finite-element analysis is employed only in certain parts of the problem domain while other parts are handled by one-dimensional (1-D) discretization following the analysis of MoL, this approach is superior to the conventional finite element analysis—in which 2-D discretization is adopted in the entire problem domain, causing a lower computational efficiency.

The remainder of this paper is organized as follows. Section II derives the formulation of the FEM–MoL analysis. In Section III, the validity of the calculated results is compared to the existing literature. Also, the computational efficiency of the proposed approach is discussed. The numerical results for a number of relevant transmission-line structures are then presented and discussed. Finally, a brief conclusion of this paper is presented in Section IV.

II. FORMULATION

To illustrate the procedure of formulating the proposed approach, the transmission-line structure as shown in Fig. 1 will be analyzed in this section. As to the structure under investigation, there appears a selectively etched dielectric substrate and the metal strips are of arbitrary cross section. Also, the structure is designed enclosing with rectangular perfect electric walls and is assumed to be uniform in the z-direction. According to the complexity of the geometries and materials, the whole structure is segmented into various regions. Regions $L1$, $L2$, and $L3$, defined in $y \in (0, y_1)$, (y_2, y_3), and (y_4, B), are composed of stratified homogeneous dielectric layers. The fields in these regions will be calculated by the MoL. On the other hand, regions $E1$ and $E2$, defined in $y \in (y_1, y_2)$ and (y_3, y_4), contain materials of complex geometry. These regions to be characterized using complex geometric/material parameters will be modeled by the FEM.

According to the discretization schemes of FEM and MoL, the entire problem domain is discretized using several elements and straight lines, as shown in Fig. 2 (the materials in the structure are not depicted for clarity). The regions $E1$ and $E2$ referred as the FEM regions and they are discretized by triangular elements. The regions $L1$, $L2$, and $L3$, which are discretized by e-lines (solid vertical lines) and h-lines (dashed vertical lines), referred as the MoL regions. Also, the interfaces between the FEM and MoL regions ($y = y_1$, y_2, y_3, and y_4, see Fig. 1) are denoted by the boundaries Γ_i ($i = 1, 2, 3, 4$). Since we are interested in modes propagating in the z-direction, it is assumed that the time-harmonic dependence and the guided-wave z-dependence of the electromagnetic fields in the structure are $\exp(j\omega t)$ and $\exp(-j\beta z)$, respectively, where ω is the angular frequency and β is the propagation constant to be determined. In what follows, Sections II-A and B briefly describe the procedures of FEM and MoL. Section II-C explains how to incorporate the solutions of MoL into those of FEM, and then system matrix equations are derived.

A. Finite-Element Matrix of FEM Regions

Referring to the FEM regions in Fig. 2, the electric field $\vec{E}$ in these regions is governed by the vector Helmholtz equation

$$\nabla \times \frac{1}{\mu_r} \nabla \times \vec{E} = k_0^2 \varepsilon_r \vec{E} \tag{1}$$

where k_0 is the wavenumber in free space and ε_r and μ_r denote the relative permittivity and relative permeability of the material, respectively. By dividing the electric field into its transverse ($\vec{E}_t$) and longitudinal (E_z) components, $\vec{E} = \vec{E}_t + \hat{z}E_z$ ($\hat{z}$ is an unit vector in the z-direction), and by adopting the variable transformation introduced in [20]–[23]

$$\vec{e}_t = \beta \vec{E}_t \quad e_z = -jE_z \tag{2}$$

the Helmholtz equation can be split into its transverse and longitudinal parts and expressed in terms of the auxiliary variables $(\vec{e}_t, e_z)$.

Following the finite-element analysis, the FEM regions are divided into a number of triangular elements. Within each element, the fields $\vec{e}_t$ and e_z are approximated by a set of first-order (linear) vectorial and nodal shape functions, respectively, that is, $\vec{e}_t = \sum_{i=1}^{3} \phi_{ti}^{(e)} \vec{N}_i^{(e)}$ and $e_z = \sum_{i=1}^{3} \phi_{zi}^{(e)} L_i^{(e)}$. The superscript (e) denotes the eth element. $\vec{N}_i^{(e)}$ and $L_i^{(e)}$ are the linear shape functions. Also, $\phi_{ti}^{(e)}$ and $\phi_{zi}^{(e)}$ are the tangential and nodal unknown expansion coefficients. Using the finite-element expansions and applying the weight residual method (WRM) [22]–[24], we then obtain the following elemental matrix equations:

$$\begin{bmatrix} \left[\boldsymbol{A}_{tt}^{(e)}\right] + \beta^2 \left[\boldsymbol{B}_{tt}^{(e)}\right] & \beta^2 \left[\boldsymbol{B}_{tz}^{(e)}\right] \\ \beta^2 \left[\boldsymbol{B}_{zt}^{(e)}\right] & \beta^2 \left[\boldsymbol{B}_{zz}^{(e)}\right] \end{bmatrix} \begin{bmatrix} \boldsymbol{\phi}_t^{(e)} \\ \boldsymbol{\phi}_z^{(e)} \end{bmatrix} + \begin{bmatrix} \boldsymbol{P}_z^{(e)} \\ \boldsymbol{P}_t^{(e)} \end{bmatrix} = 0 \tag{3}$$

where $[\boldsymbol{A}_{tt}^{(e)}]$, $[\boldsymbol{B}_{tt}^{(e)}]$, $[\boldsymbol{B}_{tz}^{(e)}]$, $[\boldsymbol{B}_{zt}^{(e)}]$, and $[\boldsymbol{B}_{zz}^{(e)}]$ are the local matrices resulted from the surface integrations of the quantities in relation to the shape functions in the weighted residual equations. The entries of these matrices are available in basic FEM texts (e.g., [22]–[24]). $\boldsymbol{\phi}_t^{(e)}$ and $\boldsymbol{\phi}_z^{(e)}$ are column vectors with components being the coefficients $\phi_{t1}^{(e)}$ to $\phi_{t3}^{(e)}$ and $\phi_{z1}^{(e)}$ to $\phi_{z3}^{(e)}$, respectively. Furthermore, the components of the column vectors $\boldsymbol{P}_z^{(e)}$ and $\boldsymbol{P}_t^{(e)}$ are given by the line integrals

$$\begin{aligned} P_{zi}^{(e)} &= -k_0\beta \oint_{\Gamma^{(e)}} \left(\vec{N}_i^{(e)} \times h_z\hat{z}\right) \cdot \hat{n}\, dl, \qquad i = 1, 2, 3 \\ P_{ti}^{(e)} &= k_0\beta^2 \oint_{\Gamma^{(e)}} \left(L_i^{(e)}\hat{z} \times \vec{h}_t\right) \cdot \hat{n}\, dl, \qquad i = 1, 2, 3 \end{aligned} \tag{4}$$

where $\Gamma^{(e)}$ represents the boundary of the element (e). The vector $\hat{n}$ denotes the outward normal unit vector to the boundary $\Gamma^{(e)}$. In (4), the auxiliary fields $\vec{h}_t$ and h_z are related to the transverse and longitudinal magnetic fields $\vec{H}_t$ and H_z via the transformation

$$\vec{h}_t = \eta_0 \vec{H}_t \quad h_z = -j\eta_0 H_z \tag{5}$$

where η_0 is the intrinsic impedance of free space.

The contributions of the line integrals depend upon the location of the integration's contour. There are three situations that occurred that need to be addressed. First, in case the contour situates at the left or right electric walls of the enclosure. Second, when it is shared between two adjacent elements. Third, if it borders at the interfaces between FEM regions and MoL regions (Γ_1, Γ_2, Γ_3, and Γ_4, in Fig. 2). For the first case, the line integral would vanish due to the boundary conditions at the conducting surfaces. As for the second occurrence, since the outward normal vectors of two adjacent elements are opposite, the contributions resulting from the two elements would annihilate each other when they are assembled. Only the line integrals of the third case should be included in the final equations. Therefore, the presence of the line integral vectors $\boldsymbol{P}_z^{(e)}$ and $\boldsymbol{P}_t^{(e)}$ are required only if the element (e) has an edge bordering at the boundary Γ_i, $(i = 1, 2, 3, 4)$. In this scenario, the line integrals over the closed contour $\Gamma^{(e)}$ can be replaced by those integrated along the edge on the boundary.

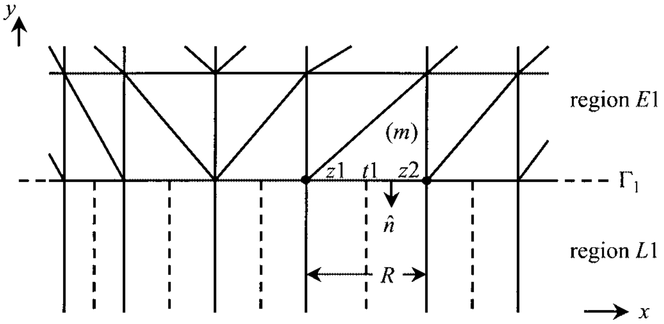

Fig. 3. Illustration of the discretization over the boundary Γ_1. The solid and dashed lines in region $L1$ are e-lines and h-lines, respectively.

To evaluate the line integrals associated with Γ_1, let us consider the element (m) shown in Fig. 3. The element (m) has an edge $t1$ located at the boundary Γ_1. Two endpoints of edge $t1$ are numbered as nodes $z1$ and $z2$. Since the outward normal vector $\hat{n}$ on edge $t1$ is $-\hat{y}$, only h_z and h_x (the tangential components of $\vec{h}$ field) are needed to perform the line integral (4) over the edge. Using the linear finite element expansions with respect to the electric fields in element (m) along with the Maxwell equations, one can approximate h_z on edge $t1$ to be a constant $\psi_z^{(m)}$, whereas h_x to be $\psi_{x1}^{(m)}$ and $\psi_{x2}^{(m)}$ at nodes $z1$ and $z2$ with linear variation along the edge. The fields h_z and h_x at edge $t1$ are then written as

$$h_z = \psi_z^{(m)} \quad h_x = \psi_{x1}^{(m)} L_1^{(m)} + \psi_{x2}^{(m)} L_2^{(m)} \tag{6}$$

where $L_1^{(m)}$ and $L_2^{(m)}$ are the nodal shape functions relative to the nodes $z1$ and $z2$ of the element (m).

Substituting (6) into (4) and using the features of the linear shape functions ($\vec{N}_2^{(m)}$ and $\vec{N}_3^{(m)}$ directed along the y-direction at edge $t1$, and $L_3^{(m)}$ vanishes along edge $t1$), the line integral vectors of the element (m) ($\boldsymbol{P}_z^{(m)}$ and $\boldsymbol{P}_t^{(m)}$) can be evaluated by performing the integrals over edge $t1$, to be expressed as

$$\begin{aligned} \boldsymbol{P}_z^{(m)} &= -k_0\beta \begin{bmatrix} R & 0 & 0 \\ 0 & 0 & 0 \\ 0 & 0 & 0 \end{bmatrix} \begin{Bmatrix} \psi_z^{(m)} \\ 0 \\ 0 \end{Bmatrix} \\ \boldsymbol{P}_t^{(m)} &= \boldsymbol{P}_x^{(m)} = -\frac{k_0\beta^2}{6} \begin{bmatrix} 2R & R & 0 \\ R & 2R & 0 \\ 0 & 0 & 0 \end{bmatrix} \begin{Bmatrix} \psi_{x1}^{(m)} \\ \psi_{x2}^{(m)} \\ 0 \end{Bmatrix} \end{aligned} \tag{7}$$

where R is the length of edge $t1$. In (7), the vector $\boldsymbol{P}_t^{(m)}$ is referred as $\boldsymbol{P}_x^{(m)}$ to indicate that it results from the field h_x at edge $t1$. The elemental matrix equations of the element (m) are then obtained by (3) and (7). Also note that in the element (m), the expansion coefficient $\phi_{t1}^{(m)} = \phi_x^{(m)}$ represents the field e_x along edge $t1$, while $\phi_{z1}^{(m)}$ and $\phi_{z2}^{(m)}$ represent e_z at nodes $z1$ and $z2$.

For other elements which have an edge adjacent to the boundary Γ_1, and those that have an edge bordering at the boundary Γ_2, Γ_3, or Γ_4, a similar treatment can be applied to calculate the elemental matrix equations. Finally, by assembling the contributions from all the elements, we can obtain a system equation for the FEM regions

$$\begin{bmatrix}[\boldsymbol{S}_{E1}] & \\ & [\boldsymbol{S}_{E2}]\end{bmatrix}\begin{Bmatrix}\begin{Bmatrix}\boldsymbol{\phi}_{\Gamma_1}\\ \boldsymbol{\phi}_{in,\,E1}\\ \boldsymbol{\phi}_{\Gamma_2}\end{Bmatrix}\\ \begin{Bmatrix}\boldsymbol{\phi}_{\Gamma_3}\\ \boldsymbol{\phi}_{in,\,E2}\\ \boldsymbol{\phi}_{\Gamma_4}\end{Bmatrix}\end{Bmatrix} + \begin{bmatrix}[\boldsymbol{C}_{E1}] & \\ & [\boldsymbol{C}_{E2}]\end{bmatrix}\begin{Bmatrix}\begin{Bmatrix}\boldsymbol{\psi}_{\Gamma_1}\\ 0\\ \boldsymbol{\psi}_{\Gamma_2}\end{Bmatrix}\\ \begin{Bmatrix}\boldsymbol{\psi}_{\Gamma_3}\\ 0\\ \boldsymbol{\psi}_{\Gamma_4}\end{Bmatrix}\end{Bmatrix} = 0 \quad (8)$$

where the submatrices $[\boldsymbol{S}_{E1}]$ ($[\boldsymbol{C}_{E1}]$) and $[\boldsymbol{S}_{E2}]$ ($[\boldsymbol{C}_{E2}]$) are the surface (line) integral matrices assembled from the contributions of the elements in the regions $E1$ and $E2$, respectively. The vectors $\boldsymbol{\phi}_{\text{in},\ E1}$ and $\boldsymbol{\phi}_{\text{in},\ E2}$ represent the unknown expansion coefficients of $\vec{e}$ field in the interior of regions $E1$ and $E2$. Also, the vector $\boldsymbol{\phi}_{\Gamma_i}$ and $\boldsymbol{\psi}_{\Gamma_i}$ ($i = 1, 2, 3, 4$) stand for the tangential components (x and z components) of $\vec{e}$ field and $\vec{h}$ field at the boundary Γ_i. $\boldsymbol{\phi}_{\Gamma_i}$ and $\boldsymbol{\psi}_{\Gamma_i}$ are written as

$$\boldsymbol{\phi}_{\Gamma_i} = \begin{Bmatrix}\boldsymbol{\phi}_{x\Gamma_i}\\ \boldsymbol{\phi}_{z\Gamma_i}\end{Bmatrix} \quad \boldsymbol{\psi}_{\Gamma_i} = \begin{Bmatrix}\boldsymbol{\psi}_{z\Gamma_i}\\ \boldsymbol{\psi}_{x\Gamma_i}\end{Bmatrix} \quad (9)$$

where the vectors $\boldsymbol{\phi}_{z\Gamma_i}$ and $\boldsymbol{\psi}_{x\Gamma_i}$ represent the values of the fields e_z and h_x at the nodes, and $\boldsymbol{\phi}_{x\Gamma_i}$ and $\boldsymbol{\psi}_{z\Gamma_i}$ represent those of the fields e_x and h_z along the line segments (edges) at Γ_i.

In the system of (8), the number of unknowns is larger than that of equations (due to the presence of unknowns ψ). Also, the unknowns are only associated with some parts (the FEM regions) of the whole problem domain. To take other parts (the MoL regions) into consideration, we next utilize the MoL to calculate the fields in the MoL regions. Another set of equations, which correlate $\boldsymbol{\phi}_{\Gamma_i}$ with $\boldsymbol{\psi}_{\Gamma_i}$, will be formulated using the solutions obtained from the MoL.

B. Field Equations of MoL Regions

The MoL regions in Fig. 1 are composed of stratified homogeneous dielectric layers. These multilayered structures can be efficiently analyzed using the MoL. The procedure for applying the MoL to multilayered structures has been discussed much in the literature. According to the formulation of this technique, the problem domain of a multilayered structure under analysis is discretized in the x-direction by several e-lines and h-lines (see the discretization schemes for the MoL regions shown in Fig. 2). The field components E_y, E_z, and H_x are then sampled at the e-lines, whereas E_x, H_y, and H_z are sampled at the h-lines. By applying several mathematical transformations, the fields in each dielectric layer of the structure are transformed into the transform domain, which can be evaluated analytically at the discrete lines [25].

With the field solutions, the transformed tangential fields ($\overline{\boldsymbol{E}}_{x,\,z}$ and $\overline{\boldsymbol{H}}_{x,\,z}$) at the lower and the upper interfaces of an arbitrary dielectric layer are related by

$$\begin{Bmatrix}\overline{\boldsymbol{H}}_a\\ \overline{\boldsymbol{H}}_b\end{Bmatrix} = \begin{bmatrix}[\overline{y}_1] & [\overline{y}_2]\\ [\overline{y}_2] & [\overline{y}_1]\end{bmatrix}\begin{Bmatrix}\overline{\boldsymbol{E}}_a\\ -\overline{\boldsymbol{E}}_b\end{Bmatrix} \quad (10)$$

with $\overline{\boldsymbol{H}}_{a,\,b} = \eta_0\{-j\overline{\boldsymbol{H}}_{za,\,b}, \overline{\boldsymbol{H}}_{xa,\,b}\}^t$, $\overline{\boldsymbol{E}}_{a,\,b} = \{\overline{\boldsymbol{E}}_{xa,\,b}, -j\overline{\boldsymbol{E}}_{za,\,b}\}^t$. Here we use the subscripts a and b to denote, respectively, the lower and the upper interfaces of the investigated layer. The transfer matrices $[\overline{\boldsymbol{y}}_1]$ and $[\overline{\boldsymbol{y}}_2]$ are defined the same as those in [25].

Using the continuity conditions of the tangential fields at the interfaces of adjacent layers, the field equations (10) of each layer are combined to correlate the tangential fields at the top boundary of the multilayered structure with those at the bottom boundary. This leads to the following equations:

$$\begin{Bmatrix}\overline{\boldsymbol{H}}_A\\ \overline{\boldsymbol{H}}_B\end{Bmatrix} = \begin{bmatrix}[\overline{\mathbf{Y}}_1] & [\overline{\mathbf{Y}}_2]\\ [\overline{\mathbf{Y}}_3] & [\overline{\mathbf{Y}}_4]\end{bmatrix}\begin{Bmatrix}\overline{\boldsymbol{E}}_A\\ -\overline{\boldsymbol{E}}_B\end{Bmatrix}. \quad (11)$$

The interface matrices $[\overline{\mathbf{Y}}_j]$ ($j = 1, 2, 3, 4$) can be readily calculated by a simple recurrence manipulation of the transfer matrices ($[\overline{\boldsymbol{y}}_1]$ and $[\overline{\boldsymbol{y}}_2]$ in (10)) for each layer [25]. The subscripts A and B denote the bottom and the top boundaries of the multilayered structure.

The field equations (11) describe the boundary conditions at the bottom and the top boundaries of a multilayered structure. It is worth noting that the interface matrices $[\overline{\mathbf{Y}}_j]$ are composed by four (quasi-)diagonal matrices. Minimal computing time and computer memory are required by this formulation. Applying MoL to investigating the MoL regions, one obtains the field equations (11) for the regions $L1$, $L2$, and $L3$. The boundary conditions at the boundaries Γ_i, $(i = 1, 2, 3, 4)$, can be then formulated from these field equations.

Before the end of this subsection, it should be pointed out that in the FEM–MoL approach, the discretization schemes for the MoL regions, that is, the positions (x-coordinates) of the e-lines and h-lines, are based on the FEM meshing on the boundaries Γ_i. The discretization applied in region $L1$ is explained here as an example. As seen in Fig. 3, the interface between regions $L1$ and $E1$ (boundary Γ_1) is divided into several line segments by finite element discretization in region $E1$. The e-lines and h-lines are placed, respectively, at the positions of endpoints and midpoint on each line segment to divide the domain of region $L1$. As illustrated in the following, this discretization schemes would appropriately incorporate the field equations of the MoL regions into the system equation of FEM regions. Similar discretization schemes can be applied to the regions $L2$ and $L3$. A nonequidistant discretization may be required in the analysis of MoL. In such a case, suitable normalization manipulations [25] should be employed in the analysis.

C. System Equations of the Whole Structure

After obtaining the field equation (11) for all MoL regions, the boundary conditions at the bottom and the top metal shieldings of the structure are inserted into (11) for regions $L1$ and $L3$, respectively. Transforming the field equations back into the spatial domain, the boundary conditions at the boundaries Γ_i are determined, which can be expressed in the form

$$\begin{aligned} \{\boldsymbol{H}_{\Gamma_1}\} &= -[\mathbf{Y}_4^{L1}]\{\boldsymbol{E}_{\Gamma_1}\} \\ \begin{Bmatrix} \boldsymbol{H}_{\Gamma_2} \\ \boldsymbol{H}_{\Gamma_3} \end{Bmatrix} &= \begin{bmatrix} [\mathbf{Y}_1^{L2}] & [\mathbf{Y}_2^{L2}] \\ [\mathbf{Y}_3^{L2}] & [\mathbf{Y}_4^{L2}] \end{bmatrix} \begin{Bmatrix} \boldsymbol{E}_{\Gamma_2} \\ -\boldsymbol{E}_{\Gamma_3} \end{Bmatrix} \\ \{\boldsymbol{H}_{\Gamma_4}\} &= [\mathbf{Y}_1^{L3}]\{\boldsymbol{E}_{\Gamma_4}\}. \end{aligned} \tag{12}$$

The matrices $[\mathbf{Y}_j^{Lk}]$, $(j = 1, 2, 3, 4$, and $k = 1, 2, 3)$ are calculated from the inverse transforming of the interface matrices ($[\overline{\mathbf{Y}}_j]$ in (11)) associated with the region Lk. The vectors $\boldsymbol{E}_{\Gamma_i}$ and $\boldsymbol{H}_{\Gamma_i}$ $(i = 1, 2, 3, 4)$ are related to the tangential fields at the boundary Γ_i with

$$\boldsymbol{E}_{\Gamma_i} = \begin{Bmatrix} \boldsymbol{E}_{x,\Gamma_i} \\ -j\boldsymbol{E}_{z,\Gamma_i} \end{Bmatrix} \quad \boldsymbol{H}_{\Gamma_i} = \eta_0 \begin{Bmatrix} -j\boldsymbol{H}_{z,\Gamma_i} \\ \boldsymbol{H}_{x,\Gamma_i} \end{Bmatrix}. \tag{13}$$

Since the field components E_z and H_x are sampled at e-lines, it is clear from the discretization schemes for the MoL regions that the components of the vectors $\boldsymbol{E}_{z,\Gamma_i}$ and $\boldsymbol{H}_{x,\Gamma_i}$ represent the fields E_z and H_x at the nodes on Γ_i (the intersections of e-lines and Γ_i). Similarly, the fields E_x and H_z are sampled at h-lines, the components of the vectors $\boldsymbol{E}_{x,\Gamma_i}$ and $\boldsymbol{H}_{z,\Gamma_i}$ thus denote the fields E_x and H_z at the middle points of the line segments, or the fields along the line segments, on Γ_i.

Next, using the variable transformation (2) and (5), the tangential fields $E_{x,z}$ and $H_{x,z}$ at the boundaries Γ_i (which are represented by the vectors $\boldsymbol{E}_{\Gamma_i}$ and $\boldsymbol{H}_{\Gamma_i}$ (13) in the MoL analysis) are transformed into the auxiliary variables $e_{x,z}$ and $h_{x,z}$ (which are represented by the vectors $\boldsymbol{\phi}_{\Gamma_i}$ and $\boldsymbol{\psi}_{\Gamma_i}$ (9) in the FEM analysis). The vectors $\boldsymbol{E}_{\Gamma_i}$ and $\boldsymbol{H}_{\Gamma_i}$ can then be expressed in terms of vectors $\boldsymbol{\phi}_{\Gamma_i}$ and $\boldsymbol{\psi}_{\Gamma_i}$ as

$$\begin{aligned} \boldsymbol{E}_{\Gamma_i} &= \begin{Bmatrix} \boldsymbol{E}_{x,\Gamma_i} \\ -j\boldsymbol{E}_{z,\Gamma_i} \end{Bmatrix} = \begin{Bmatrix} \beta^{-1}\boldsymbol{\phi}_{x,\Gamma_i} \\ \boldsymbol{\phi}_{z,\Gamma_i} \end{Bmatrix} = [\boldsymbol{Q}]\{\boldsymbol{\phi}_{\Gamma_i}\} \\ \boldsymbol{H}_{\Gamma_i} &= \begin{Bmatrix} -j\eta_0\boldsymbol{H}_{z,\Gamma_i} \\ \eta_0\boldsymbol{H}_{x,\Gamma_i} \end{Bmatrix} = \begin{Bmatrix} \boldsymbol{\psi}_{z,\Gamma_i} \\ \boldsymbol{\psi}_{x,\Gamma_i} \end{Bmatrix} = \boldsymbol{\psi}_{\Gamma_i} \\ [\boldsymbol{Q}] &= \begin{bmatrix} \beta^{-1}[\boldsymbol{I}] & 0 \\ 0 & [\boldsymbol{I}] \end{bmatrix} \end{aligned} \tag{14}$$

where $[\boldsymbol{I}]$ is the unit matrix. Substituting (12) and (14) into (8), we finally obtain the following nonstandard eigenvalue equation to the problem:

$$[\boldsymbol{F}(\beta)]\{\phi\} = 0. \tag{15}$$

In order to get nontrivial solutions for the coefficient vector $\boldsymbol{\phi}$, the determinant of system matrix $[\boldsymbol{F}]$ should be zero. By solving the determinantal equation via various root searching algorithms such as the Muller's method or the singular value decomposition technique [26], the propagation constants β are obtained. With β already known, all guided fields are explicitly calculable, and other electric characteristics (e.g., the impedance) can be further computed.

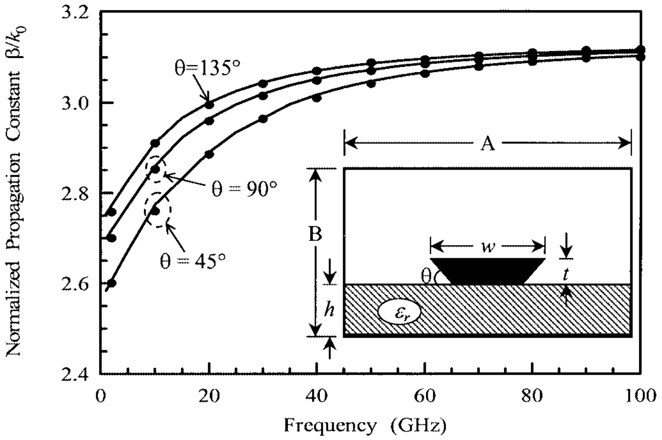

Fig. 4. Normalized propagation constant as a function of frequency for a thick microstrip structure. Structural parameters are $\mathrm{A} = 10.0$ mm, $\mathrm{B} = 6.985$ mm, $w = 3.0$ mm, $h = 0.635$ mm, $t = 0.3$ mm, and $\varepsilon_r = 9.8$. Lines: FEM–MoL approach. Dots: Alam *et al.* [7].

In the FEM–MoL analysis of this example, the problem domain is segmented into two FEM and three MoL regions. For the analysis of a more complex structure, additional FEM and MoL regions can be applied. The equations of the FEM regions and those of the MoL regions can be combined using the procedure described above to acquire the system equations to the problem.

III. NUMERICAL RESULTS

In this section, the numerical results for a variety of transmission-line structures are presented. For all examples considered, the media are assumed lossless, isotropic, and nonmagnetic ($\mu_r = 1$). Also, nonuniform discretization schemes that refinedly discrete the areas in which the fields can change rapidly by smaller elements and/or closer spaced lines are employed in the analyses.

To validate the proposed formulation, a thick microstrip structure with rectangular or trapezoidal metallization cross section (see the inset of Fig. 4) is investigated to compare our results with those available in the existing literature. Fig. 4 shows the propagation characteristics of the rectangular strip ($\theta = 90°$) and those of the trapezoidal ones ($\theta = 45°$ and 135°). The results obtained from our approach (represented by the solid lines) are in excellent agreement with those calculated by Alam *et al.*using a standard finite-element approach [7] (marked by the dots). In the FEM–MoL analysis, the FEM region is defined in $y \in (h, h+t)$, i.e., the layer containing the metal strip. The substrate layer ($y \in (0, h)$) and the air layer above the metal strip ($y \in (h + t, B)$) are defined as MoL regions. Note that the FEM region (which is handled by 2-D discretization) occupies only about 4.29% of the whole problem domain. It is expected that the computational performance of the proposed approach would be much more efficient than that of the conventional finite element method (in which 2-D discretization is adopted to the entire problem domain).

In order to investigate the computational performance of the FEM–MoL analysis, the convergence property of this technique in analyzing the microstrip structure with rectangular metal strip considered in Fig. 4 at 20 GHz is examined and compared with

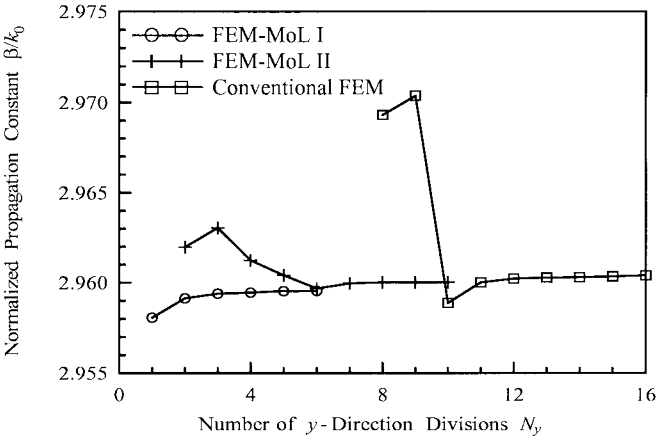

Fig. 5. Convergence properties of the normalized propagation constants computed by the FEM–MoL and conventional FEM analyses. The structure under test is the microstrip structure with a rectangular metal strip shown in Fig. 4 at 20 GHz. The number of divisions in the x -direction N_x is 78 for all three analyses.

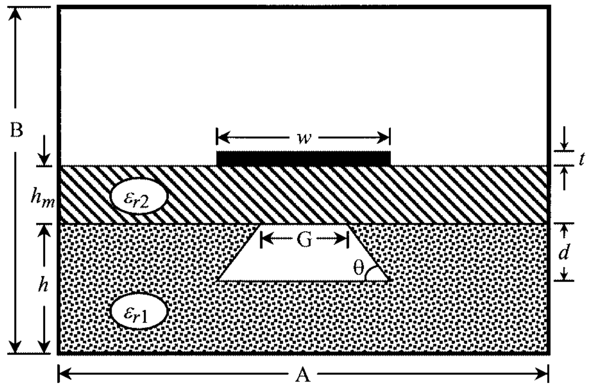

Fig. 6. Membrane-supported microstrip line.

that of the conventional FEM. Two FEM–MoL formulations, referred as FEM–MoL I and FEM–MoL II, are implemented in the convergence study to reveal the flexibility of this method. In FEM–MoL I, the problem domain is segmented into one FEM ($y \in (h, h+t)$) and two MoL ($y \in (0, h)$ and $(h+t, B)$) regions. While in FEM–MoL II, two FEM ($y \in (2t/3, 5t/3)$ and $(h, h+t)$) and three MoL ($y \in (0, 2t/3)$, $(5t/3, h)$, and $(h+t, B)$) regions are used. The conventional FEM can be treated as a special FEM–MoL implementation of which the whole problem domain is defined as the FEM region since it uses the finite element method to handle the whole structure. In the calculation, the FEM regions of each implementation are first divided into $N_x \times N_y$ rectangular elements, where N_x and N_y are the number of divisions in the x- and y-directions. Each rectangular element is later divided into two triangular elements. The MoL regions (for FEM–MoL I and II analyses) are then discretized by lines according to the discretizing procedure stated in Section II-B. Under these discretization schemes, the number of variables computed in the FEM–MoL I, II, and the conventional FEM are, respectively, $4N_xN_y+2N_x-2N_y-1$, $4N_xN_y+4N_x-2N_y-2$, and $4N_xN_y-2N_x-2N_y+1$ (including the variables associated with the fields on the metal strip, which can be excluded when the strip is treated as a PEC).

Fig. 5 presents the convergence curves of the normalized propagation constants as a function of N_y. The data of these three implementations are calculated using the same x-direction discretization pattern with $N_x = 78$ (which has been found to be large enough to achieve the convergence with respect to N_x for all three analyses). As can be seen in the graph, the curves of the three analyses converge to the same value ($\beta/k_0 \approx 2.960$). However, the FEM–MoL technique requires fewer y-direction divisions to converge the data than does the conventional FEM. The converged result is achieved with at least 11 y-direction divisions through the conventional FEM, whereas the same result can be obtained by the FEM–MoL I using only three y-direction divisions. This clearly indicates that a much fewer number of variables are needed to obtain an accurate result by using the FEM–MoL technique. In this example, the number of variables computed in the FEM–MoL I after eliminating those on the metal strip is about 20% of that in the conventional FEM. Due to the decrease of the number of variables, the computing time is reduced. Nevertheless, it should be mentioned that in the conventional FEM the problem can be formulated as a standard eigenvalue problem with the propagation constant being the eigenvalue, whereas the FEM–MoL approach will result in a determinantal matrix equation since the propagation constant cannot be factored from the matrices accounted for the MoL regions. Also, unlike the finite-element analysis that would lead to a sparse matrix, the system matrix resulting from the FEM–MoL technique is partly sparse and partly full. Some efficient matrix techniques [20], [24] that are usually adopted in the finite-element analysis to improve the computational efficiency would be therefore no longer applicable in the FEM–MoL technique.

In the following, a microstrip line with an air cavity underneath the supporting membrane is considered. The configuration of the membrane-supported microstrip line is illustrated in Fig. 6, where an air cavity is etched on a silicon substrate using micromachining techniques [9], [10], [12], [17]. The sidewalls of the cavity are aligned to the $\langle 111 \rangle$ silicon crystal planes with the sidewall angle θ being 54.7° [12]. In the FEM–MoL analysis of this structure, the region containing the air cavity ($y \in (h-d, h)$) and that containing the metal strip ($y \in (h+h_m, h+h_m+t)$) are defined as the FEM regions. Other parts of the structure are specified as the MoL regions.

Fig. 7 presents the effective dielectric constants of the membrane-supported microstrip line. The results obtained from the case without an air cavity (G $= 0$) are also presented in Fig. 7 for comparison. The arrows along with the plot are used to indicate the increase of cavity depth d. The increment of either the cavity width G or the depth d results in the reduction of the effective dielectric constants because the electric field in the silicon substrate is reduced. Furthermore, the air cavity is observed to improve the dispersive propagation characteristics of the microstrip. The dependence of the propagation characteristics on frequency decreases apparently as the cavity size (G or d) is increased. In the case of G $= 2w$, the effective dielectric constants are nearly independent to the operating frequency, indicating that the membrane-supported lines have almost zero dispersion. Although not shown here, it has also been found that when the cavity width G increases to an extent

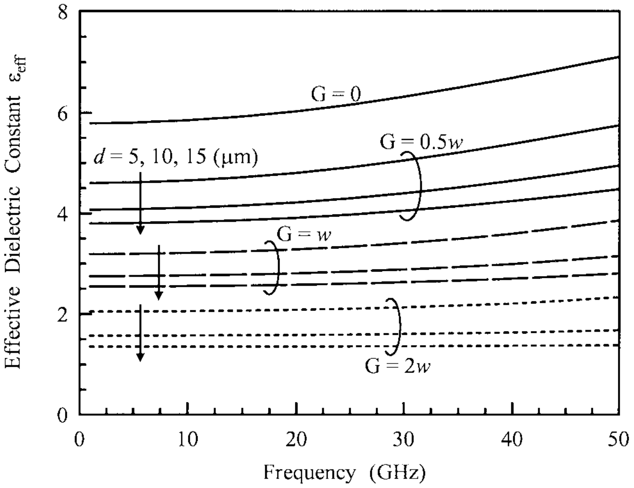

Fig. 7. Effective dielectric constant as a function of frequency for a membrane-supported microstrip line. Structural parameters are in Fig. 6, $A = 1.2$ mm, $w = 0.2$ mm, $h = 0.3$ mm, $h_m = 0.005$ mm, $t = 0.001$ mm, $B = 0.605$ mm, $\varepsilon_{r1} = 11.7$, $\varepsilon_{r2} = 4$, and $\theta = 54.7°$.

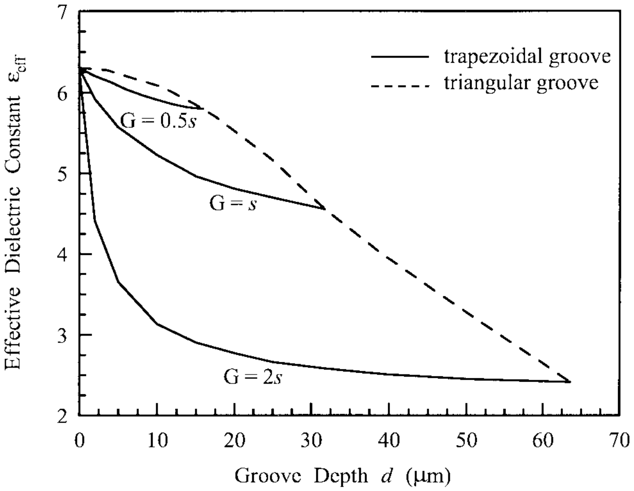

Fig. 9. Effective dielectric constant as a function of groove depth for a micromachined coplanar waveguide. Structural parameters are in Fig. 8, $A = 0.32$ mm, $B = 0.5$ mm, $w = 0.05$ mm, $s = 0.045$ mm, $h = 0.3$ mm, $t = 0.001$ mm, $\varepsilon_r = 11.7$, and $\theta = 54.7°$.

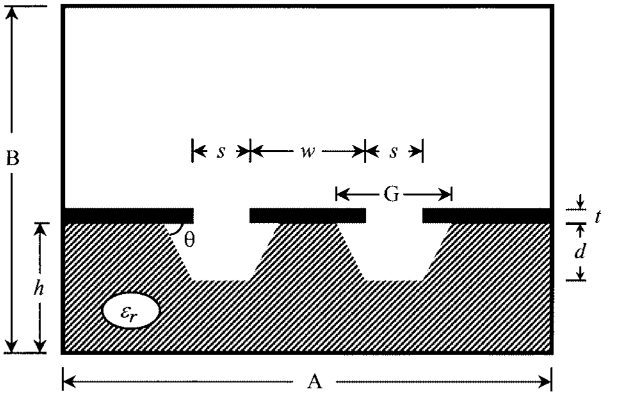

Fig. 8. Micromachined coplanar waveguide.

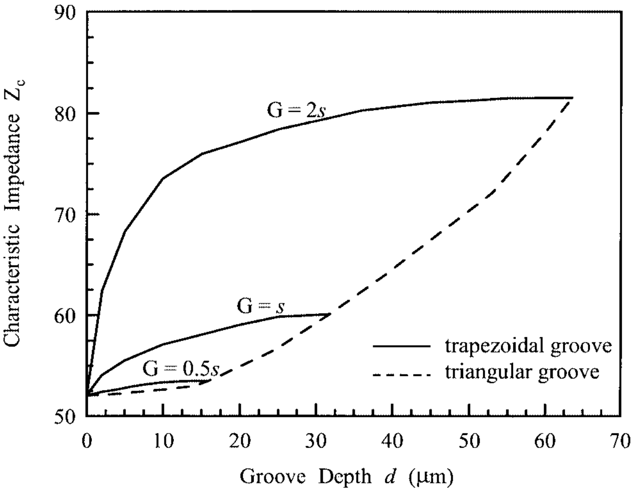

Fig. 10. Characteristic impedance as a function of groove depth for a micromachined coplanar waveguide. Structural parameters are in Fig. 8, $A = 0.32$ mm, $B = 0.5$ mm, $w = 0.05$ mm, $s = 0.045$ mm, $h = 0.3$ mm, $t = 0.001$ mm, $\varepsilon_r = 11.7$, and $\theta = 54.7°$.

larger than the strip width w at a given cavity depth d, the effective dielectric constant tends to converge to a stable value. When G is larger than $2w$, the effective dielectric constant remains nearly unchanged after further increase in G. This reflects the fact that most of the fields concentrate in the region underneath the strip.

As a final example, let us consider a micromachined coplanar waveguide [13], [17] packaged in a metallic enclosure. Fig. 8 depicts the structure to be studied. In this line, the silicon materials in area underneath the apertures between the conductors are removed by wet etching using EDP (anisotropic etch) or HF/Nitric (isotropic etch) [9], [10], [13], [17]. As a result, an air groove is formed below the aperture. The sidewall angle of the air groove θ is 54.7°. In the FEM–MoL analysis, the FEM and MoL regions are, respectively, defined in $y \in (h-d,\ h+t)$ and $y \in (0,\ h-d)$, $(h+t,\ B)$.

Since the electric fields concentrate in the apertures between the conductors, the removal of the materials underneath the apertures would lower the effective dielectric constant. Furthermore, the lower effective dielectric constant can lead to a lower line capacitance that increases the characteristic impedance [17]. Figs. 9 and 10 demonstrate the influence of the air grooves on the effective dielectric constant and the characteristic impedance, respectively. In both figures, the solid lines represent the results for the cases of the groove with trapezoidal cross sections (isotropically etched profile), and the dashed line represents those for the cases of the triangular groove (anisotropically etched profile). There are three isotropic cases with different groove widths ($\mathrm{G} = 0.5s$, s, and $2s$) to be considered here. Also, the groove width G for the anisotropic case depends on the groove depth d with an angle of 54.7°.

For the cases of trapezoidal groove, it can be seen that the effective dielectric constant decreases and the characteristic impedance increases with increasing groove depth d. When the depth d approaches the limit value of $(\mathrm{G}/2)\tan(54.7°)$, the characteristic values tend to converge to those relating to the case of triangular groove. Also, it is noticed that when the groove width G is larger than the aperture width s, the characteristic values would change drastically as the groove depth d

increases by a small amount from $d = 0$. In regard to the cases of triangular groove, the effective dielectric constant decreases and the characteristic impedance increases monotonously when the depth (thus the width) of the groove is enlarged.

IV. CONCLUSION

A full-wave approach incorporating the FEM and the MoL has been presented to efficiently analyze a planar or quasi-planar transmission-line structure containing complex geometric/material features. In this work, when a transmission-line structure is analyzed, the complex regions in the structure are modeled by the FEM, while the simple regions are analyzed using the MoL. Using the field solutions obtained from the MoL, the boundary conditions are constructed and utilized to carry out the boundary integrals involved in finite-element analysis. It not only retains the major advantage of finite element method in modeling complex structures but also is more efficient than the conventional finite element analysis. The validity of the present approach was confirmed by conducting the comparative study as well as the convergence analysis. Moreover, good computational efficiency of this method was observed from the convergence property of this method. Finally, the propagation characteristics of membrane-supported microstrip lines and micromachined coplanar waveguides were also investigated and demonstrated with satisfactory applicability.

REFERENCES

[1] J. J. Kucera and R. J. Gutmann, "Effect of finite metallization and inhomogeneous dopings on slow-wave-mode propagation," *IEEE Trans. Microwave Theory Tech.*, vol. 45, pp. 1807–1810, Oct. 1997.

[2] K. Wu and R. Vahldieck, "Propagation characteristics of MIS transmission lines with inhomogeneous doping profile," *IEEE Trans. Microwave Theory Tech.*, vol. 38, pp. 1872–1878, Dec. 1990.

[3] S. Chen, R. Vahldieck, and J. Huang, "Rigorous analysis of mode propagation and field scattering in silicon-based coplanar MIS slow wave structures with abrupt transitions to transmission lines on normal substrate," *IEEE Trans. Microwave Theory Tech.*, vol. 44, pp. 2487–2494, Dec. 1996.

[4] J.-F. Kiang, "Quasi-TEM analysis of coplanar waveguides with an inhomogeneous semiconductor substrate," *IEEE Trans. Microwave Theory Tech.*, vol. 44, pp. 1586–1589, Sept. 1996.

[5] L. Zhu and E. Yamashita, "Effects of conductor edge profile on transmission properties of conductor-backed coplanar waveguides," *IEEE Trans. Microwave Theory Tech.*, vol. 43, pp. 847–853, Apr. 1995.

[6] J.-T. Kuo and T. Itoh, "Hybrid-mode computation of propagation and attenuation characteristics of parallel coupled microstrips with finite metallization thickness," *IEEE Trans. Microwave Theory Tech.*, vol. 45, pp. 274–280, Feb. 1997.

[7] M. S. Alam, K. Hirayama, Y. Hayashi, and M. Koshiba, "Analysis of shielded microstrip lines with arbitrary metallization cross section using a vector finite element method," *IEEE Trans. Microwave Theory Tech.*, vol. 42, pp. 2112–2117, Nov. 1994.

[8] F.-L. Lin and R.-B. Wu, "Analysis of coplanar-waveguide discontinuities with finite-metallization thickness and nonrectangular edge profile," *IEEE Trans. Microwave Theory Tech.*, vol. 45, pp. 2131–2138, Dec. 1997.

[9] S. V. Robertson, A. R. Brown, L. P. B. Katehi, and G. M. Rebeiz, "A 10–60-GHz micormachined directional coupler," *IEEE Trans. Microwave Theory Tech.*, vol. 46, pp. 1845–1849, Nov. 1998.

[10] S. V. Robertson, L. P. B. Katehi, and G. M. Rebeiz, "Micormachined W-band filters," *IEEE Trans. Microwave Theory Tech.*, vol. 44, pp. 598–606, Apr. 1996.

[11] M. Ozgur, V. Milanović, C. Zincke, M. Gaitan, and M. E. Zaghloul, "Quasi-TEM characteristic impedance of micromachined CMOS coplanar waveguides," *IEEE Trans. Microwave Theory Tech.*, vol. 48, pp. 852–854, May 2000.

[12] V. Milanović, M. Gaitan, E. D. Bowen, and M. E. Zaghloul, "Micromachined microwave transmission lines in CMOS technology," *IEEE Trans. Microwave Theory Tech.*, vol. 45, pp. 630–635, May 1997.

[13] K. J. Herrick, T. A. Schwarz, and L. P. B. Katehi, "Si-micromachined coplanar waveguides for use in high-frequency circuits," *IEEE Trans. Microwave Theory Tech.*, vol. 46, pp. 762–768, June 1998.

[14] Y. Yan and P. Pramanick, "Finite-element analysis of generalized V- and W-shaped edge and broadside-edge-coupled shielded microstrip lines on anisotropic medium," *IEEE Trans. Microwave Theory Tech.*, vol. 49, pp. 1649–1657, Sept. 2001.

[15] Y. Kwon, H. T. Kim, J. H. Park, and Y. K. Kim, "Low-loss micromachined inverted overlay CPW lines with wide impedance ranges and inherent airbridge connection capability," *IEEE Microwave Wireless Comp. Lett.*, vol. 11, pp. 59–61, Jan. 2001.

[16] H. T. Kim, S. Jung, J. H. Park, C. W. Baek, Y. K. Kim, and Y. Kwon, "A new micromachined overlay CPW structure with low attenuation over wide impedance ranges and its application to low-pass filters," *IEEE Trans. Microwave Theory Tech.*, vol. 49, pp. 1634–1639, Sept. 2001.

[17] K. J. Herrick, J.-G. Yook, and L. P. B. Katehi, "Microtechnology in the development of three-dimensional circuits," *IEEE Trans. Microwave Theory Tech.*, vol. 46, pp. 1832–1844, Nov. 1998.

[18] J.-F. Kiang, "Capacitance of microstrip lines with inhomogeneous substrate," *IEEE Trans. Microwave Theory Tech.*, vol. 44, pp. 1703–1709, Oct. 1996.

[19] ——, "Microstrip lines on substrates with segmented or continuous permittivity profiles," *IEEE Trans. Microwave Theory Tech.*, vol. 45, pp. 229–235, Feb. 1997.

[20] J. F. Lee, D. K. Sun, and Z. J. Cendes, "Full-wave analysis of dielectric waveguides using tangential vector finite elements," *IEEE Trans. Microwave Theory Tech.*, vol. 39, pp. 1262–1271, Aug. 1991.

[21] J. F. Lee, "Finite element analysis of lossy dielectric waveguides," *IEEE Trans. Microwave Theory Tech.*, vol. 42, pp. 1025–1031, June 1994.

[22] G. Pelosi, R. Coccioli, and S. Selleri, *Quick Finite Elements for Electromagnetic Waves*. Norwood, MA: Artech House, 1998.

[23] J. M. Jin, *The Finite Element Method in Electromagnetics*. New York: Wiley, 1993.

[24] J. L. Volakis, A. Chatterjee, and L. C. Kempel, *Finite Element Method for Electromagnetics*. Piscataway, NJ: IEEE Press, 1998.

[25] R. Pregla and W. Pascher, "The method of lines," in *Numerical Techniques for Microwave and Millimeter Wave Passive Structures*, T. Itoh, Ed. New York: Wiley, 1989, ch. 6.

[26] V. A. Labay and J. Bornemann, "Matrix singular value decomposition for pole-free solutions of homogeneous matrix equations as applied to numerical modeling methods," *IEEE Microwave Guided Wave Lett.*, vol. 2, pp. 49–51, Feb. 1992.

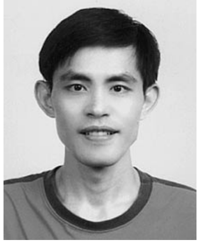

Hao-Hui Chen (M'99) was born in Kaohsiung, Taiwan, R.O.C., on April 11, 1969. He received the B.S. degree in physics from the National Central University, Taoyuan, Taiwan, R.O.C., in 1991, and the Ph.D. degree in communication engineering from the Nation Chiao Tung University, Hsinchu, Taiwan, R.O.C., in 1998.

Since 1998, he has been with the Department of Electronic Engineering, Huafan University, Taipei, Taiwan, R.O.C., where he is currently an Assistant Professor. His research interests include computational electromagnetics, microwave integrated circuits and packages, as well as microelectromechanical microwave circuits.